High-resolution imaging of intravascular atherogenic inflammation in live mice

Raphael Chèvre PhD, Jose María González-Granado PhD*, Remco T.A. Megens PhD*, Vinatha Sreeramkumar PhD, Carlos Silvestre-Roig PhD, Pedro Molina-Sánchez BS, Christian Weber MD, Oliver Soehnlein MD PhD, Andrés Hidalgo PhD** and Vicente Andrés PhD**

From the Department of Epidemiology, Atherothrombosis and Imaging, Centro Nacional de Investigaciones Cardiovasculares, Madrid, Spain (R.C., J.M.G.-G., V.S., C.S.-R., P.M-S., A.H. and V.A.); Institute for Cardiovascular Prevention, Ludwig-Maximilians-University Munich and DZHK (German Centre for Cardiovascular Research), partner site Munich Heart Alliance, Munich, Germany (R.T.A.M., C.W., O.S.); Cardiovascular Research Institute Maastricht, the Netherlands (R.T.A.M., C.W.); Academic Medical Center Amsterdam, University of Amsterdam, the Netherlands (O.S.).

Correspondence to Andrés Hidalgo or Vicente Andrés, Centro Nacional de Investigaciones Cardiovasculares, Department of Epidemiology, Atherothrombosis and Imaging, Melchor Fernández Almagro 3, 28029 Madrid, Spain. Phone: +34 91-4531200. E-mail ahidalgo@cnic.es or vandres@cnic.es

* J.M.G.-G. and R.T.A.M. contributed equally to this work.
** V.A. and A.H. contributed equally as corresponding and senior authors

Abstract

Rationale: The inflammatory processes that initiate and propagate atherosclerosis remain poorly understood, largely because defining the intravascular behavior of immune cells has been technically challenging. Respiratory and pulsatile movements have hampered *in vivo* visualization of leukocyte accumulation in athero-prone arteries at resolutions achieved in other tissues.
Objective: To establish and to validate a method that allows high resolution imaging of inflammatory leukocytes and platelets within the carotid artery of athero-susceptible mice *in vivo*.
Methods and results: We have devised a procedure to mechanically stabilize the mouse carotid artery without altering blood dynamics, which dramatically enhances temporal and spatial resolutions using high-speed intravital microscopy in multiple channels of fluorescence. By applying this methodology at different stages of disease progression in athero-susceptible mice, we first validated our approach by assessing the recruitment kinetics of various leukocyte subsets and platelets in athero-prone segments of the carotid artery. The high temporal and spatial resolution allowed the dissection of both the dynamic polarization of and formation of subcellular domains within adhered leukocytes. We further demonstrate that the secondary capture of activated platelets on the plaque is predominantly mediated by neutrophils. Finally, we couple this procedure with triggered two-photon microscopy to visualize the three-dimensional movement of leukocytes in intimate contact with the arterial lumen.
Conclusions: The improved imaging of diseased arteries at subcellular resolution presented here should help resolve many outstanding questions in atherosclerosis and other arterial disorders.

Subject codes: [134] Atherosclerosis / Pathophysiology – [150] Atherosclerosis / Imaging – [97] Other Vascular biology – [61] Vascular imaging / Other imaging

Key Words: Intravital microscopy – two-photon microscopy – atherosclerosis – platelets – *in vivo* imaging – neutrophils – carotid artery

Nonstandard Abbreviations and Acronyms:

ApoE$^{-/-}$: apolipoprotein E-null mice
APC: Allophycocyanin
HFD: High-fat diet
FITC: Fluorescein isothiocyanate
PE: Phycoerythrin
TPLSM: Two-photon laser scanning microscopy

Introduction

Atherosclerosis is a chronic inflammatory disease of large arteries and a major cause of mortality in Western societies.[1] Immune cells and platelets are considered important mediators of all phases of atherosclerosis, from the initial asymptomatic lesions to the establishment of complex vulnerable plaques that can rupture and provoke acute ischemic events (e.g., myocardial infarction or stroke) and associated disability and mortality.[2, 3] Different subsets of leukocytes accumulate in atherosclerotic lesions and contribute to the maturation and destabilization of the plaque.[4, 5] Particularly important are blood-borne monocytes, which accumulate in the injured arterial wall after interacting with dysfunctional endothelial cells and differentiate into macrophages, which ultimately propagate inflammation within the atherosclerotic plaque.[5, 6] Less abundant in the plaque, but also important mediators at specific stages of atherosclerosis, are neutrophils and B and T lymphocytes.[4, 5] On the luminal side of the plaque, neutrophils and platelets promote disease progression by releasing chemoattracting factors and other intracellular material.[7-10] However, the absence of reliable tools for real-time visualization of leukocytes, platelets or other thrombo-inflammatory mediators within affected arteries at high resolution severely limits our understanding of how intravascular inflammation drives atherogenesis.

Multiple genetic models and immunohistological tools have been used to dissect key aspects of the etiopathogenesis of atherosclerosis, but they have not provided sufficient insight into the question of leukocyte accumulation and behavior at the endothelial interphase. Attempts to directly image leukocyte recruitment in athero-prone regions by applying epifluorescent or two-photon laser scanning microscopy (TPLSM) in explanted arteries have yielded important mechanistic information on the processes that underlie disease progression, including a role of adhesion receptors in leukocyte recruitment,[11] accumulation of activated platelets[8] or local presentation of antigens by dendritic cells to T-lymphocytes.[12] Whilst these studies with explanted arteries dramatically improved image quality, they have failed to provide the complex rheological and immune context present in the arterial lumen of live animals. It is also noteworthy that application of real-time imaging in live mice to visualize atherogenic arteries (e.g., aorta and carotid arteries) has been challenged by the respiratory and pulsatile movements of these vessels, which greatly limited the temporal and spatial resolution of live imaging and prevented analysis of the dynamics of leukocytes and platelets in the atherogenic environment, or the identification of subcellular structures.[11, 13-15] Thus, key questions related to the recruitment of different leukocyte subsets, their activation and migration on and across the injured endothelium, and the formation of multicellular aggregates that are well characterized in the microvasculature of many tissues[8, 16, 17] remain to be answered in the context of atherosclerosis.

Here, we sought to establish an easy to apply and reliable imaging methodology for *in vivo* visualization of dynamic processes during atherogenesis at subcellular and sub-second resolutions. We report a procedure to stabilize the carotid artery of live mice that dramatically reduces spontaneous vertical movements of the vessel generated by the heart cycle and respiration, without causing significant alterations of the physiological blood flow. Combined with high-speed multichannel epifluorescence and TPLSM platforms, the method enables visualization of inflammatory phenomena within the lumen of the artery at high spatial and temporal resolutions in up to four dimensions. We have used this system to image intra-luminal events in athero-prone Apolipoprotein E-null mice ($ApoE^{-/-}$) at different stages of disease and combined it with reporter genes and fluorescent probes to track various subsets of inflammatory cells and subcellular structures *in vivo*.

Methods

For detailed Materials and Methods, please see the Online Data Supplement.

Mice. Mafia:*ApoE*$^{-/-}$ mice were generated by crossing ApoE$^{-/-}$ (Charles River, Lyon, France) with Mafia mice, which express GFP under the control of the *c-fms* promoter.[18] Alternatively, *Lysm*$^{egfp/egfp}$*ApoE*$^{-/-}$ mice[19] were used to visualize neutrophils. All mice were in the C57BL/6J background and were housed in a pathogen-free barrier facility. For diet-induced atherosclerotic studies, 6-8 week-old male mice were fed an atherogenic high fat diet (HFD: 10.8% total fat, 0.75% cholesterol, S8492-E010, Ssniff, Germany) for the indicated periods of time. All experimental protocols were approved by the local authorities for animal experimentation.

Surgical preparation and stabilization of the carotid artery. Mice were anesthetized with a mixture of ketamine (Imalgene 1000; Merial, France) and medetomidine (Medeson; Urano, Spain) (50 mg/kg and 0.5 mg/kg, respectively). Surgical preparation and stabilization of the carotid artery for imaging are described in Result section (Figure 1) and online supplemental material.

Results

Preparation of the carotid artery for stabilized imaging

The bifurcation of the common left carotid artery is susceptible to atherosclerosis in humans and mice and is easily accessible with minor surgery. We therefore chose this region to develop a procedure that allowed vessel stabilization without significantly compromising blood flow for subsequent high-resolution *in vivo* imaging. Mice were anesthetized, placed in *decubitus* position, and the carotid artery exposed and carefully dissected without disrupting the surrounding muscular tissues or nerves[7] (Figure 1A). To isolate the vessel from the respiratory motions of the thorax we placed a beveled flat metal piece under the vessel (Figure 1B). This bottom metallic support was attached to a rigid pole that was immobilized on a lateral holder. To reduce the pulsatile movements of the artery caused by the cardiac cycles, an image-grade round coverslip 12 mm in diameter was cut in half, placed over the artery and flexibly fixed to the bottom support using modeling clay (Figure 1C). This set-up allowed us to restrain the z-motion of the arterial wall by gently pressing on the coverslip to obtain a separation of 400±50 μm between both supports. The stabilized region of the artery was then placed under the objective of a multichannel epifluorescence microscope with constant perfusion of warm saline buffer (Figure 1D). This simple preparation yielded a ~1 mm-long segment of the common carotid artery and the two branches of the bifurcation in which vertical displacement due to thoracic and pulsatile movements was dramatically reduced compared with non-stabilized carotid arteries (Figure 2A, B, Online Movie I). We quantified stabilization by determining the Pearson's coefficient of the in-focus region of control and stabilized arteries that compared the fluorescent signal between consecutive frames captured at 5 Hz (i.e., 5 frames per second). These analyses revealed higher Pearson's coefficient in stabilized preparations (Figure 2C and Online Figure I). Although some lateral movement was still present in mechanically-stabilized arteries, the use of epifluorescent illumination allowed continued imaging of the structures of interest over time and facilitated off-line analyses. Notably, the stability of the tissue was comparable to that obtained with the well-established cremaster muscle model (Online Figure IB-C), which has been extensively used to study inflammation in the microvasculature.[17, 20]

To assess whether the stabilizing procedure altered the hemodynamics of the carotid artery, we injected 1 μm fluorescent beads and measured velocities at low magnification. We found little perturbations in blood flow dynamics (Figure 2D and Online Movie II), with diastolic velocities of 4.4 ± 0.6 cm/s that are consistent with those reported using ECG-gated magnetic resonance imaging.[21]

For subsequent imaging of atherosclerotic regions within the living carotid artery, we chose regions proximal to the bifurcation, in areas where plaques developed over time under pro-atherogenic conditions (Figure 2E, F and Online Movie III). In these areas, the stabilization procedure allowed efficient imaging of defined intravascular structures even at high magnification (Online Movie IV). We thus set out to validate this method for visualization of atherogenic inflammation.

Leukocyte dynamics in atherogenic regions

We first imaged the stabilized carotid artery at low magnification in athero-susceptible mice deficient in ApoE$^{-/-}$. Animals were fed standard diet or challenged with an atherogenic HFD for 2 or 4 weeks and then intravenously injected with rhodamine 6G to label luminal cells, and with fluorescent beads coated with anti-VCAM-1 antibodies to identify regions with dysfunctional endothelium (Figure 3A, B). The VCAM-1-coated beads, but not control rIgG-coated beads (Online Figure II), predominantly accumulated at the level of the bifurcation in fat-fed mice, and this correlated with large

foci of rolling and adherent leukocytes in the same areas (Figure 3B). In contrast, leukocytes and VCAM-1 were both largely absent from areas outside the bifurcation in fat-fed mice or from the arteries of mice fed with standard chow (Figure 3A-B). Leukocyte recruitment was also largely absent from small arteriolar vessels of the cremasteric microcirculation of HFD-treated mice (Online Figure III). Thus, inflammation and the ensuing recruitment of leukocytes in the visualized carotid artery is specifically induced by the atherogenic diet, rather than by surgical manipulation.

To obtain high temporal and spatial resolutions (up to 9.2 Hz and ≈0.6 μm), we next captured images using a 40x NA 1.0 objective in a single-channel of fluorescence of the carotid artery of fat-fed ApoE$^{-/-}$ mice. Rhodamine labeling revealed high numbers of rolling leukocytes at the bifurcation as early as 2 weeks post-HFD, which increased at 4 weeks (Figure 3C-G and Online Movie V), whereas virtually no recruitment was seen under non-atherogenic standard conditions (Figure 3C, D, G).

Luminal recruitment of leukocytes appeared to be the major way of recruitment during early atherosclerosis since at these stages we could not detect *vasa vasora*, contrary to their reported abundance in late-stage atheromata.[22] The high temporal resolution of our acquisitions further allowed measurement of leukocyte rolling velocities, which decreased upon fat-feeding over time and inversely correlated with the number of rolling cells (Figure 3G, H).

Identification of leukocyte subsets recruited to atherosclerotic lesions

Multiple leukocyte subsets contribute to atherosclerosis by triggering diverse innate and acquired immune processes.[4, 5] To assess the specific recruitment of various leukocyte subsets in the atherogenic artery, we took advantage of Mafia reporter mice which allow easy identification of GFP+ circulating monocytes and neutrophils.[18] Analysis of ApoE$^{-/-}$ mice expressing the Mafia transgene (Mafia:ApoE$^{-/-}$) revealed a robust recruitment of myeloid cells as early as 10 days post-HFD (Figure 4A), with elevated numbers of rolling and adherent GFP+ cells at the carotid bifurcation (Online Movie VI). In these experiments, many GFP+ cells were already present at the time of imaging, and we could estimate that 2.1% (9 out of 430) of the myeloid cells that came rolling transitioned into firm arrest at the bifurcation. Interestingly, timestamp analyses revealed preferential areas of leukocyte rolling (Online Figure IVA), suggesting heterogeneous activation of endothelial cells within the same arterial regions.

In order to simultaneously track the behavior of distinct leukocyte subsets, we injected Mafia:ApoE$^{-/-}$ mice with fluorescently-tagged antibodies against CD4, CD8 and Ly6G, using doses (0.4 to 1 μg/mouse) that do not significantly alter leukocyte behavior *in vivo*.[20, 23] We took advantage of the fast filter-change system of our intravital microscopy setup to acquire images in three channels of fluorescence for near-simultaneous identification of CD4/CD8+ T cells, Ly6G^{HI} GFP+ neutrophils and Ly6G$^{NEG/LO}$ GFP+ monocytes recruited to the carotid bifurcation after 2 and 6 weeks on HFD (Figure 4B). These analyses revealed increased numbers of rolling neutrophils over time, whereas that of monocytes was similar at both time points (Figure 4C)
Interestingly, despite the progressive reduction in the relative amount of circulating T-lymphocytes in fat-fed mice (Online Figure IVB, C), rolling of these cells was only detected after 6 weeks post-HFD (Figure 4C), suggesting that activated T-cell subsets appear only at later stages of disease development. Analysis of the rolling dynamics of the different cell subsets revealed that neutrophils display high but similar rolling velocities at both time points, while the rolling velocity of monocytes was markedly reduced after 6 weeks on HFD (Figure 4C). These observations reveal different kinetics of recruitment for monocytes, neutrophils and T lymphocytes during atherogenesis, and a more efficient (i.e., slower rolling velocities) recruitment of monocytes as disease progresses.

Intravascular polarization and crawling of myeloid leukocytes

In the inflamed microcirculation, leukocyte recruitment proceeds through distinct phases.[24] After rolling, leukocytes firmly adhere to the endothelium and this is followed by a rapid change in their morphology and redistribution of specific receptors to defined microdomains, a process known as polarization.[20, 25] In late stages, polarized neutrophils crawl on the endothelium in search of areas permissive for extravasation.[26] To determine whether leukocyte polarization and crawling also occur in atherosclerotic vessels, we tracked the behavior of adhered myeloid GFP+ leukocytes at the carotid bifurcation of fat-fed Mafia:ApoE$^{-/-}$ mice. Before imaging, mice were injected with a fluorescently-conjugated anti-L-selectin (CD62L) antibody to allow identification of the uropod in polarized leukocytes.[17] Using this strategy, we identified a small fraction of GFP+ neutrophils that transitioned from rolling to arrest, underwent morphological polarization, and redistributed CD62L to the cell's uropod (Figure 5A and Online Movie VII). The spatio-temporal resolution of the images allowed quantification of rolling and crawling velocities (Figure 5B, C), as well as tracking of CD62L redistribution in polarizing cells (Figure 5D, E). The CD62L-enriched uropod could be detected in many GFP+ cells crawling along the arterial endothelium, some of which moved against the direction of the flow, away from landmark structures present in the plaque (Figure5B, Online Movie VII). We also observed that a fraction of crawling cells left tracks of CD62L-immunoreactive material on the endothelium (Online Figure V). These structures were not artifacts generated by the residual lateral motion of the preparation, as they were maintained over time with the same morphology (not shown). These observations demonstrate that leukocyte recruitment to atherosclerotic lesions follows the same fundamental phases described in the microvasculature, and further reveal the feasibility of *in vivo* visualization of subcellular structures within inflamed large arteries.

Accumulation of activated platelets in atherosclerotic lesions requires interaction with recruited myeloid cells

Activated platelets have been associated with the development of atherosclerosis. Binding of platelets to both myeloid and endothelial cells has been proposed to promote leukocyte recruitment through deposition of inflammatory chemokines.[8, 27, 28] Thus, we next examined the mechanisms by which platelets are recruited to atherosclerotic lesions *in vivo*. To this end, we injected fat-fed Mafia:ApoE$^{-/-}$ mice with a fluorescently-conjugated anti-CD41 antibody which allows specific detection of platelets in vivo (Online Figure VI).[17] Microscopic fields were divided in three categories: "*Low adhesion"* (absence or very low presence of adherent GFP+ myeloid cells), "*Myeloid clusters"* (strong presence of singly adherent GFP+ cells and small autofluorescent structures), and "*Lesion shoulder"* (presence of three dimensional structures and GFP+ cells). We found that few platelets bound to the endothelium in areas devoid of leukocytes (Online Movie VIII), and instead preferentially bound to adherent GFP+ myeloid leukocytes present in the periphery of established plaques (lesion shoulders) (Figure 6A and Online Movie IX). Depletion of circulating myeloid cells with an anti-Gr-1 (anti-Ly6G/C) antibody almost completely abolished platelet accumulation, as did specific depletion of neutrophils with an anti-Ly6G antibody (Figure 6B, Online Figure VII). These data indicate that the initial accumulation of neutrophils precedes and mediates platelet accumulation in the lumen of atherosclerotic arteries.

To determine the activation state of platelets that accumulated around arrested leukocytes, and to further examine their interactions with myeloid leukocytes *in vivo*, we performed 4-channel imaging of GFP, Ly6G and CD41 together with a fluorescently-conjugated JON/A antibody (Online Movie X), which recognizes the active form of the

αIIbβ3 integrin present in activated platelets[29]. We confirmed that platelets bound to GFP+ cells (both Ly6G-positive and negative), and found that the activation epitope marked preferentially small thrombi associated with lesion shoulders (Figure 6C-E and Online Movie X). These analyses indicate that activated platelets are dynamically recruited to the developing atheroma and that they do so by interacting with previously adhered monocytes and neutrophils.

Visualization of myeloid cell dynamics in 3D over time

As a proof of principle, we also visualized myeloid cell dynamics using TPLSM, an optical imaging method with superior depth discrimination enabling multidimensional imaging but also suffering severely from the impact of motion of a sample.[15, 30] We applied TPLSM to visualize myeloid cells recruitment in fat-fed *Lysm*$^{egfp/egfp}$ApoE$^{-/-}$ mice. Even if application of the stabilizer tool strongly reduced the impact of both cardiac and respiratory movement, additional triggering on the respiratory cycle further limited the impact of respiratory movement artifacts, thereby yielding better image quality and stability. This synchronization ultimately allowed us to acquire multidimensional datasets over prolonged times (Figure 7A-D, Online Movies XI and XII). Individual myeloid cell movement along the arterial lumen could be studied in a relatively large field of view (450x450µm; Figure 7B and Online Movie XI), in which we noted rapid changes in the shape of polarized cells as well as changes in their directionality of crawling. Intravenous application of 150 kDa TRITC-Dextran allowed for better discrimination between lumen and vessel wall (Figure 7D, Online Movie XII), revealing that the cells were firmly adherent to the arterial wall, flattened and migrated in clusters along the lumen (Figure 7B). Moreover, image processing enabled volume rendering and provided a spatial context of the leukocyte, the vessel wall, and the lumen (Figure 7C, E); it also provided detailed kinetics in 3D of single and clustered leukocytes (Figure 7F, Online Movie XIII). These TPLSM analyses demonstrate the feasibility of high-resolution imaging of inflammatory cells in up to four dimensions within atherosclerotic arteries *in vivo*.

Discussion

In this study we have developed a surgical procedure that stabilizes the carotid artery without significant alterations in flow dynamics that enabled high-resolution imaging of atherosclerotic lesions in live mice. We have applied wide-field fluorescence and TPLSM microscopy to the stabilized artery at different stages of atherogenesis. We show for the first time the feasibility of subsecond and submicron imaging of atherogenic inflammation in the presence of physiological flow, which allowed us to make several new observations: first, we dissect the kinetics and dynamics of recruitment of various subpopulations of inflammatory leukocytes, and show that this process is an early event during atherogenesis. Second, we identify the presence of activated platelets in established atherosclerotic plaques, and show that platelet incorporation into the injured wall largely relies on the presence of neutrophils. Finally, we show that the degree of arterial stabilization is sufficient for two-photon microscopy-driven multidimensional imaging of leukocyte-vessel wall interactions.

Important for these imaging analyses of inflammatory cell behavior during atherosclerosis was the use of different myeloid GFP-based reporter models in an ApoE$^{-/-}$ background. We have shown that the use of these reporter mice in combination with fluorescent probes allows efficient visualization of myeloid leukocytes, subcellular structures and platelet dynamics. Other molecules and cells of interest during atherosclerosis can be visualized with this technology by using multiple fluorescent probes that are commercially available (e.g., antibodies or fluorogenic substrates), as well as other reporter murine strains. For example, it should be possible to examine the specific recruitment and behavior of regulatory and interleukin 17-producing T cells, patrolling or inflammatory populations of monocytes, neutrophils or platelets during atherosclerosis using existing reporter mice.[31-34].

Direct visualization of exposed carotid arteries at low magnification previously allowed analysis of leukocyte rolling[14] or identification of cellular clusters, but visualization at higher resolution or in 3D was prevented by the pulsatile motion of the arterial wall. Synchronization of acquisition with arterial wall motion allowed nonetheless an increase in spatial resolution in the z-axis at the cost of temporal resolution.[15] In contrast, other studies in which the artery was fully immobilized allowed imaging of the arterial wall at high spatial resolution, but completely abrogated the physiological blood flow and could not be used to study the dynamic inflammatory events that occurred intravascularly.[35] Here, by stabilizing the vessel in the vertical plane and using epifluorescent illumination, we tracked dynamic events at high resolution despite the persistence of residual XY movements. This approach yielded a high temporal resolution in several channels of fluorescence, and thus the possibility to track the dynamics of various cells populations in the arterial wall. Using subset-specific markers, we could estimate rolling frequencies and velocities for monocytes, neutrophils and T lymphocytes within the same vessels. Notably, although the use of epifluorecence and the large size of the vessel limits imaging to the upper side of the artery, and may exclude other areas of interest (e.g., the branching point at the bifurcation fork), our data demonstrates the feasibility and utility of the approach to investigate thrombo-inflammatory events in areas where leukocytes accumulate and plaques form.

Another limitation of the method is the persistence of lateral movements of the vessel due to the compression of the artery against the stabilizing surfaces and residual respiratory movement; nonetheless, we show the stabilization to be sufficient for two-photon imaging when combined with respiration-triggered acquisition. This improvement allowed, for the first time, detailed analyses in 3D of the intravascular lesion over time and revealed clusters of neutrophils crawling in intimate contact with the endothelium. Caution should also be exerted with the choice of anesthetics used

for mouse preparation, as some mixtures may result in alterations in global hemodynamics[36], and may introduce potential alterations in the behavior of inflammatory leukocytes and platelets in the atherogenic artery.

Using these new tools, we show that myeloid cell recruitment to the injured arterial wall occurs very early during atherogenesis. Whereas the role of monocytes and macrophages is widely accepted,[37] neutrophils have only recently been recognized to participate in disease progression.[38] The observation that platelet recruitment is favored by neutrophils already present in the atherosclerotic lumen, reconciles the established roles of platelet-derived factors[8] with the pro-atherogenic functions of neutrophils in the early stages of the disease.[13] We also demonstrate that leukocyte recruitment in injured areas occurs through the same fundamental steps reported in the microvasculature,[24] with cells transitioning from rolling to firm arrest, with subsequent polarization and crawling on the endothelium. Interestingly, interactions between platelets and polarized neutrophils have been associated to other forms of acute vascular inflammation,[17] and may underlie the initial stages of endothelial damage associated with atherosclerosis.

Altogether, these findings illustrate the potential of this approach to study relevant thrombo-inflammatory events that may occur during atherogenesis, including the recruitment of microparticles,[39] formation of thrombi,[40] or the deposition of DNA-based structures from activated neutrophils.[9] Identification of subcellular domains on leukocytes and small luminal CD62L+ debris suggests that the method should be also useful to study the role of small biological structures (e.g., lipid deposits, cellular microdomains or apoptotic bodies) in atherosclerosis. We propose that this approach will be instrumental for the study of the thrombo-inflammatory phenomena that underlie atherosclerosis and other forms of arterial disease.

Novelty and Significance

What Is Known?

- Atherosclerosis is an inflammatory process of large arteries that originates and perpetuates by the pathological accumulation of myeloid cells and platelets into the injured artery.
- The recruitment of leukocytes to inflamed areas occurs through a series of sequential steps that are well characterized in the microcirculation.
- Respiratory and pulsatile movements have prevented dissection of intravascular inflammation of atherogenic arteries using high-resolution imaging.

What New Information Does This Article Contribute?

- Mechanical stabilization of the carotid artery allows imaging atherogenic inflammation within the vessel at high-resolution in live mice.
- Multichannel imaging allows simultaneous dissection of the kinetics and dynamics of recruitment of monocytes, T lymphocytes and neutrophils to the atherogenic lesion; it further reveals a requirement for neutrophils in platelet accumulation.
- The method allows 3-dimensional (3D) imaging of the atherogenic artery by multiphoton microscopy.

The extreme motility of athero-prone arteries prevents imaging of inflammatory processes at resolutions achieved in other tissues. We present a method to stabilize the carotid artery without major effects on intravascular hemodynamics that results in dramatic enhancement of image resolution. Using multiple fluorescent probes and reporter mice, the method provided a detailed analysis of the different stages of leukocyte recruitment within the atherogenic arteries of live mice. Further imaging revealed subcellular reorganization of receptors in recruited leukocytes and showed that the accumulation of platelets is mediated by neutrophils previously recruited to the lesion. This set up also facilitated the application of multiphoton microscopy to obtain 3D reconstructions of leukocytes moving on the atherosclerotic endothelium over time. Our method of high-resolution in vivo imaging of atherogenic arteries opens new possibilities to dissect the mechanisms underlying atherosclerosis and other arterial disorders.

Acknowledgements. We thank V. Zorita, I. Ortega, C. Pitaval, M. Nus and the Cellomics, Microscopy and Comparative Medicine Units at CNIC for gift of reagents, technical support and animal care. We also thank L. Weiss for critically reviewing and editing the manuscript, Ben Atkinson for technical help with intravital microscopy platform, Dr. Villa-Bellosta for photography, and A. de Andrés for artwork.

Sources of Funding. Work in the authors' laboratories is supported by grants from the Spanish Ministry of Economy and Competitivity (MINECO) (SAF2009-11037, SAF2010-16044), the European Commission (FP7-People-IRG 246655, Liphos-317916), and Instituto de Salud Carlos III (RD12/0042/0028). A.H. is supported by a Ramón y Cajal fellowship (RYC-2007-00697) and J.M.G-G. by the ISCIII Miguel Servet program (CP11/00145). O.S. is supported by the NWO (VIDI project 91712303), the DFG (SO876/3-1, SO876/6-1, FOR809, SFB914-B08), the Else Kröner Fresenius Stiftung, and the LMUexcellence initiative. R.T.A.M. and C.W. were supported by DFG (FOR809, WE1913/11-2, KI 1072/8-1, LMUexcellence initiative) and European Research Council (ERC AdG°249929). The TPLSM was supported by the DFG (INST409/97-1) and the Friedrich Baur Stiftung. The Centro Nacional de Investigaciones Cardiovasculares (CNIC) is supported by the MINECO and the Pro-CNIC Foundation.

Author Contributions. R.C. performed experiments and wrote the manuscript; J.M.G-G., V.S.,C.S. and P.M-S. performed experiments; C.W, O.S. and R.T.A.M. performed two-photon microscopic data acquisition, data analysis and manuscript writing. A.H. and V.A. conceived the study and wrote the manuscript.

Author Information. Correspondence and requests for materials should be addressed to A.H. or V.A. (ahidalgo@cnic.es; vandres@cnic.es).

Competing financial interests
The authors declare no competing financial interests.

References

1. Roger VL, Go AS, Lloyd-Jones DM, Adams RJ, Berry JD, Brown TM, Carnethon MR, Dai S, de Simone G, Ford ES, Fox CS, Fullerton HJ, Gillespie C, Greenlund KJ, Hailpern SM, Heit JA, Ho PM, Howard VJ, Kissela BM, Kittner SJ, Lackland DT, Lichtman JH, Lisabeth LD, Makuc DM, Marcus GM, Marelli A, Matchar DB, McDermott MM, Meigs JB, Moy CS, Mozaffarian D, Mussolino ME, Nichol G, Paynter NP, Rosamond WD, Sorlie PD, Stafford RS, Turan TN, Turner MB, Wong ND, Wylie-Rosett J. Heart disease and stroke statistics--2011 update: a report from the American Heart Association. *Circulation.*123(4):e18-e209.

2. Binder CJ, Chang MK, Shaw PX, Miller YI, Hartvigsen K, Dewan A, Witztum JL. Innate and acquired immunity in atherogenesis. *Nat Med.* 2002;8(11):1218-1226.

3. Huo Y, Ley KF. Role of platelets in the development of atherosclerosis. *Trends in cardiovascular medicine.* 2004;14(1):18-22.

4. Galkina E, Ley K. Leukocyte influx in atherosclerosis. *Current drug targets.* 2007;8(12):1239-1248.

5. Weber C, Noels H. Atherosclerosis: current pathogenesis and therapeutic options. *Nat Med.* 2011;17(11):1410-1422.

6. Libby P, Ridker PM, Hansson GK. Progress and challenges in translating the biology of atherosclerosis. *Nature.* 2011;473(7347):317-325.

7. Doring Y, Drechsler M, Wantha S, Kemmerich K, Lievens D, Vijayan S, Gallo RL, Weber C, Soehnlein O. Lack of neutrophil-derived CRAMP reduces atherosclerosis in mice. *Circ Res.* 2012;110(8):1052-1056.

8. Huo Y, Schober A, Forlow SB, Smith DF, Hyman MC, Jung S, Littman DR, Weber C, Ley K. Circulating activated platelets exacerbate atherosclerosis in mice deficient in apolipoprotein E. *Nat Med.* 2003;9(1):61-67.

9. Megens RT, Vijayan S, Lievens D, Doring Y, van Zandvoort MA, Grommes J, Weber C, Soehnlein O. Presence of luminal neutrophil extracellular traps in atherosclerosis. *Thromb Haemost.* 2012;107(3):597-598.

10. Zernecke A, Bot I, Djalali-Talab Y, Shagdarsuren E, Bidzhekov K, Meiler S, Krohn R, Schober A, Sperandio M, Soehnlein O, Bornemann J, Tacke F, Biessen EA, Weber C. Protective role of CXC receptor 4/CXC ligand 12 unveils the importance of neutrophils in atherosclerosis. *Circulation research.* 2008;102(2):209-217.

11. Ramos CL, Huo Y, Jung U, Ghosh S, Manka DR, Sarembock IJ, Ley K. Direct demonstration of P-selectin- and VCAM-1-dependent mononuclear cell rolling in early atherosclerotic lesions of apolipoprotein E-deficient mice. *Circ Res.* 1999;84(11):1237-1244.

12. Koltsova EK, Garcia Z, Chodaczek G, Landau M, McArdle S, Scott SR, von Vietinghoff S, Galkina E, Miller YI, Acton ST, Ley K. Dynamic T cell-APC interactions sustain chronic inflammation in atherosclerosis. *J Clin Invest.* 2012;122(9):3114-3126.

13. Drechsler M, Megens RT, van Zandvoort M, Weber C, Soehnlein O. Hyperlipidemia-triggered neutrophilia promotes early atherosclerosis. *Circulation.* 2010;122(18):1837-1845.

14. Eriksson EE, Xie X, Werr J, Thoren P, Lindbom L. Direct viewing of atherosclerosis in vivo: plaque invasion by leukocytes is initiated by the endothelial selectins. *FASEB J.* 2001;15(7):1149-1157.

15. Megens RT, Kemmerich K, Pyta J, Weber C, Soehnlein O. Intravital imaging of phagocyte recruitment. *Thromb Haemost.* 2011;105(5):802-810.

16. Clark SR, Ma AC, Tavener SA, McDonald B, Goodarzi Z, Kelly MM, Patel KD, Chakrabarti S, McAvoy E, Sinclair GD, Keys EM, Allen-Vercoe E, Devinney R,

Doig CJ, Green FH, Kubes P. Platelet TLR4 activates neutrophil extracellular traps to ensnare bacteria in septic blood. *Nature medicine.* 2007;13(4):463-469.

17. Hidalgo A, Chang J, Jang JE, Peired AJ, Chiang EY, Frenette PS. Heterotypic interactions enabled by polarized neutrophil microdomains mediate thromboinflammatory injury. *Nat Med.* 2009;15(4):384-391.

18. Burnett SH, Kershen EJ, Zhang J, Zeng L, Straley SC, Kaplan AM, Cohen DA. Conditional macrophage ablation in transgenic mice expressing a Fas-based suicide gene. *J Leukoc Biol.* 2004;75(4):612-623.

19. Rotzius P, Soehnlein O, Kenne E, Lindbom L, Nystrom K, Thams S, Eriksson EE. ApoE(-/-)/lysozyme M(EGFP/EGFP) mice as a versatile model to study monocyte and neutrophil trafficking in atherosclerosis. *Atherosclerosis.* 2009;202(1):111-118.

20. Chiang EY, Hidalgo A, Chang J, Frenette PS. Imaging receptor microdomains on leukocyte subsets in live mice. *Nat Methods.* 2007;4(3):219-222.

21. Parzy E, Miraux S, Franconi JM, Thiaudiere E. In vivo quantification of blood velocity in mouse carotid and pulmonary arteries by ECG-triggered 3D time-resolved magnetic resonance angiography. *NMR Biomed.* 2009;22(5):532-537.

22. Eriksson EE. Intravital microscopy on atherosclerosis in apolipoprotein e-deficient mice establishes microvessels as major entry pathways for leukocytes to advanced lesions. *Circulation.* 2011;124(19):2129-2138.

23. Yipp BG, Kubes P. Antibodies against neutrophil LY6G do not inhibit leukocyte recruitment in mice in vivo. *Blood.* 2013;121(1):241-242.

24. Ley K, Laudanna C, Cybulsky MI, Nourshargh S. Getting to the site of inflammation: the leukocyte adhesion cascade updated. *Nat Rev Immunol.* 2007;7(9):678-689.

25. Barreiro O, de la Fuente H, Mittelbrunn M, Sanchez-Madrid F. Functional insights on the polarized redistribution of leukocyte integrins and their ligands during leukocyte migration and immune interactions. *Immunol Rev.* 2007;218:147-164.

26. Phillipson M, Heit B, Colarusso P, Liu L, Ballantyne CM, Kubes P. Intraluminal crawling of neutrophils to emigration sites: a molecularly distinct process from adhesion in the recruitment cascade. *J Exp Med.* 2006;203(12):2569-2575.

27. Lievens D, von Hundelshausen P. Platelets in atherosclerosis. *Thromb Haemost.* 2011;106(5):827-838.

28. Koenen RR, von Hundelshausen P, Nesmelova IV, Zernecke A, Liehn EA, Sarabi A, Kramp BK, Piccinini AM, Paludan SR, Kowalska MA, Kungl AJ, Hackeng TM, Mayo KH, Weber C. Disrupting functional interactions between platelet chemokines inhibits atherosclerosis in hyperlipidemic mice. *Nat Med.* 2009;15(1):97-103.

29. Bergmeier W, Schulte V, Brockhoff G, Bier U, Zirngibl H, Nieswandt B. Flow cytometric detection of activated mouse integrin alphaIIbbeta3 with a novel monoclonal antibody. *Cytometry.* 2002;48(2):80-86.

30. Megens RT, Reitsma S, Prinzen L, oude Egbrink MG, Engels W, Leenders PJ, Brunenberg EJ, Reesink KD, Janssen BJ, ter Haar Romeny BM, Slaaf DW, van Zandvoort MA. In vivo high-resolution structural imaging of large arteries in small rodents using two-photon laser scanning microscopy. *J Biomed Opt.* 2010;15(1):011108.

31. Auffray C, Fogg D, Garfa M, Elain G, Join-Lambert O, Kayal S, Sarnacki S, Cumano A, Lauvau G, Geissmann F. Monitoring of blood vessels and tissues by a population of monocytes with patrolling behavior. *Science.* 2007;317(5838):666-670.

32. Esplugues E, Huber S, Gagliani N, Hauser AE, Town T, Wan YY, O'Connor W, Jr., Rongvaux A, Van Rooijen N, Haberman AM, Iwakura Y, Kuchroo VK, Kolls JK, Bluestone JA, Herold KC, Flavell RA. Control of TH17 cells occurs in the small intestine. *Nature.* 2011;475(7357):514-518.

33. Faust N, Varas F, Kelly LM, Heck S, Graf T. Insertion of enhanced green fluorescent protein into the lysozyme gene creates mice with green fluorescent granulocytes and macrophages. *Blood.* 2000;96(2):719-726.

34. Zhang J, Varas F, Stadtfeld M, Heck S, Faust N, Graf T. CD41-YFP mice allow in vivo labeling of megakaryocytic cells and reveal a subset of platelets hyperreactive to thrombin stimulation. *Exp Hematol.* 2007;35(3):490-499.

35. Yu W, Braz JC, Dutton AM, Prusakov P, Rekhter M. In vivo imaging of atherosclerotic plaques in apolipoprotein E deficient mice using nonlinear microscopy. *J Biomed Opt.* 2007;12(5):054008.

36. Janssen BJ, De Celle T, Debets JJ, Brouns AE, Callahan MF, Smith TL. Effects of anesthetics on systemic hemodynamics in mice. *Am J Physiol Heart Circ Physiol.* 2004;287(4):H1618-1624.

37. Weber C, Zernecke A, Libby P. The multifaceted contributions of leukocyte subsets to atherosclerosis: lessons from mouse models. *Nat Rev Immunol.* 2008;8(10):802-815.

38. Soehnlein O. Multiple roles for neutrophils in atherosclerosis. *Circ Res.* 2012;110(6):875-888.

39. Myers DD, Hawley AE, Farris DM, Wrobleski SK, Thanaporn P, Schaub RG, Wagner DD, Kumar A, Wakefield TW. P-selectin and leukocyte microparticles are associated with venous thrombogenesis. *J Vasc Surg.* 2003;38(5):1075-1089.

40. Falati S, Gross P, Merrill-Skoloff G, Furie BC, Furie B. Real-time in vivo imaging of platelets, tissue factor and fibrin during arterial thrombus formation in the mouse. *Nat Med.* 2002;8(10):1175-1181.

Figures legends

Figure 1. Surgical preparation and stabilization of the carotid artery. (A-C) Numbers indicate the different elements and tissues involved in the procedure. (**A**) Mice are immobilized in *decubitus* position and the carotid artery exposed. The salivary gland (**1**) is fixed above the preparation and hyoidei muscles surrounding carotid artery are separated and fixed with sutures (white arrows). Detail of hyoidei muscles: Omohyoid muscle (**2**), mastoid part of sternocephalic muscle (**3**), sternothyroid muscle (**4**). (**B**) Positioning of the metal support and glass coverslip for stabilization of the artery. The right vague nerve (**9**) was carefully separated from the carotid artery (**10**). A flat metal piece with a beveled edge (**6**) was placed under the vessel, while the other side of the piece was fixed to a lateral holder (**8**). Finally, an image-grade round coverslip cut in half (**5**) was placed over the artery and flexibly fixed to the bottom support using insoluble modeling clay (**7**). (**C**) Schematic representations of the stabilizer and tissues. (**D**) Image of the mouse prepared for observation under the microscope.

Figure 2. Image stability and blood dynamics. (**A, B**) Intravital microscopy of non-stabilized (A) and stabilized (B) carotid artery. The images show sequential images obtained under a 10x or 40x objectives at 5.7 and 3 Hz, respectively. Scale bar: 200 µm (10x) or 40 µm (40x). See also **Online Movie I**. (**C**) Pearson's co-localization coefficient from the 10x acquisitions of stabilized and non-stabilized arteries. (**D**) Blood flow pattern within the stabilized carotid artery, obtained by imaging free-flowing fluorescent beads (red) at low magnification. Background autofluorescence of the arterial wall appears in green. Scale bars: 100 µm See also **Online Movie II**. (**E**) Intravital microscopy of the stabilized carotid artery presenting atheroma at its bifurcation level. HFD-fed Mafia:ApoE$^{-/-}$ (8 weeks) mouse was injected intravenously with rhodamine 6G to label luminal cells (i.e, endothelial cells and leukocytes, red). GFP positive extravasated myeloid cells (green) accumulate at the bifurcation level of the carotid artery. Scale bars: 200 µm. See also **Online Movie III**. (**F**) 3D reconstruction of whole-mounted carotid artery from HFD fed Mafia:ApoE$^{-/-}$ mouse (6 weeks). Red signal shows autofluorescent arterial wall and green signal shows GFP positive myeloid cells. GFP positive extravasated cells accumulate at the bifurcation level of carotid artery. Scale bars: 200 µm.

Figure 3. High-resolution imaging of leukocyte recruitment during atherogenesis. ApoE$^{-/-}$ mice fed standard diet **(A)** or HFD (2 weeks) **(B)** were injected with rhodamine 6G (red) and anti-VCAM-1-coated fluorescent beads (green) before imaging the stabilized carotid artery. Dashed lines delimit carotid walls on the one hand, regions of leukocyte recruitment and VCAM-1 expression on the other hand. Images were obtained under a 10x objective. Scale bar: 100µm. (**C**-**F**) High-resolution images of rhodamine-labeled cells within the carotid artery of mice fed standard diet (C, D) or HFD (4 weeks; E,F). Images were obtained at the level of the common carotid (D, F) or the bifurcation (C, E). Scale bar, 20µm. See also **Online Movie V**. (**G**) Number of rolling leukocytes (left axis, black) in the carotid bifurcation (black squares) and common carotid artery (empty squares), and rolling velocity in carotid bifurcation (right axis, red) of mice fed standard chow or HFD for 2 and 4 weeks. Bars represent mean ± s.e.m. from n=6-16 fields and 16-121 leukocytes from 3-4 mice. (**H**) Correlation between the number of rolling cells and rolling velocities in the fields analyzed in (G). Bars show mean ± s.e.m. Grey arrows in A-F show the direction of flow.

Figure 4. Simultaneous tracking of leukocyte subsets recruited to atherogenic lesions. Mafia:ApoE$^{-/-}$ mice were injected with fluorescently-conjugated antibodies against CD4/CD8 and Ly6G before analysis. Arrows in A and B show the direction of flow. (**A**) Representative images of myeloid leukocytes (green) rolling at the bifurcation of the carotid artery in mice fed standard chow or HFD for ten days. Scale bars, 25 µm. See also **Online Movie VI**. (**B**) Representative images of GFP+ myeloid cells, GFP+ Ly6G+

neutrophils and GFP^{NEG} CD4/CD8+ T lymphocytes in the carotid bifurcation of mice fed HFD for 2 or 6 weeks. Images were acquired at 1.7 Hz under a 40x objective. Dashed lines delimit the lesion shoulder. Scale bars, 20 μm. (**C**) Number of rolling neutrophils (red), monocytes (green) and T lymphocytes (blue). n=18-33 fields from 4 mice. Right graph shows rolling velocity of neutrophils (red) and monocytes (green). n=33-94 neutrophils and 9-35 monocytes from 4 mice. Lines show mean ± s.e.m., ***P*<0.01, ****P*<0.001.

Figure 5. Polarization and crawling of myeloid leukocytes recruited to atherogenic lesions. Mafia:ApoE$^{-/-}$ mice on HFD for 3 weeks were injected with a fluorescently-conjugated antibody to CD62L to allow *in vivo* visualization of myeloid cell polarization. (**A**) Sequence showing CD62L distribution (white) on myeloid cells (green). The orange arrowhead points to leukocyte that arrests, polarizes and completely redistributes CD62L to the uropod within 4 min. Another polarized cell is shown crawling against the blood flow (red arrowheads). In enlarged images of the framed regions, yellow dashed lines identify polarizing and crawling leukocytes, purple dashed line indicates non polarized state and purple continued line indicates polarized state. Grey arrows show the direction of flow. Images were acquired at 2.5Hz. Scale bars, 20 μm. See also **Online Movie VII**. (**B**) Tracks of rolling and crawling leukocytes. Note that while all rolling cells follow the flow (indicated by the grey arrow), several crawling cells move against the flow. (**C**) Distances and velocities of single cells rolling (black) or crawling (red) on the endothelium. (**D**) Quantification of CD62L distribution along the axis of polarized or non-polarized leukocytes (purple dashed and continued lines in (A), respectively). (**E**) Kinetics of CD62L redistribution in the polarizing cell shown in (A). The graph shows the CD62L+ area expressed as a percentage of total leukocyte area over time.

Figure 6. Platelet recruitment to atherosclerotic lesions. Mafia:ApoE$^{-/-}$ mice were fed HFD for one month and injected with a fluorescently-conjugated antibody against CD41, and images were acquired during at least 40 s. Representative images panels show myeloid leukocytes (green) and platelets (red). White arrowheads indicate platelets. Scale bars, 20μm (A, B). (**A**) Representative images from regions devoid of leukocytes (left panel), regions with clusters of GFP+ myeloid cells (middle panel), and in lesion shoulders (right panel). See also **Online Movies VIII and IX**. Graph shows quantification of adhered platelets in different regions. n=7-12 fields from 4-7 mice. Bars show mean ± s.e.m. ****P*<0.001. (**B**) Representative images of lesion shoulders from control mice (left panel), Ly6G depleted mice (middle panel) and Ly6G/C depleted mice (right panel). Graph shows quantification of adhered platelets in depleted groups respective to the rIgG-injected group. n=10-21 fields from 3 mice. Bars show mean ± s.e.m. ****P*<0.001. (**C**) Mice prepared as in (A) were additionally injected with fluorescently-conjugated antibodies recognizing the activated β3-integrin (clone JON/A) and Ly6G before imaging. Images were acquired in four channels of fluorescence at 1Hz under a 10x objective. Scale bar, 100 μm. (**D**) Patched-composition of the region shown in (C), with images acquired using a 40x objective. Scale bar, 20 μm. (**E**) Enlarged merged image of the region shown in (D), showing also single fluorescence channels (right panels). The β3-activation epitope associates to CD41+ thrombi (orange arrowhead) that appear associated to GFP+ myeloid cells in lesion shoulders. GFP+ Ly6G-positive neutrophils (blue arrowhead) and GFP+ Ly6G–negative monocytes can be identified. The dashed line delimits the contour of the lesion in this arterial segment, also shown in (C). Scale bar, 20 μm.

Figure 7. Three dimensional (3D) imaging of atherogenic arteries over time. Two-photon microscopic imaging of the stabilized carotid artery of *Lysm$^{egfp/egfp}$ApoE$^{-/-}$* mice presented over time as 2D using extended depth of field projections, where the total Z information of each z-stack is projected in one XY image representing a total thickness

of approximately 20µm (B, D) or as 3D reconstructions (C, E, F). (**A**) Overview of recording sites within the carotid artery: the yellow box identifies regions imaged in B, C; the purple box identifies the area imaged in D, E, F. ECM, extracellular matrix. (**B**) Time series of z-stacks projected in two dimensions revealing myeloid cells (green) rolling (yellow arrow heads) and crawling (red box) on the vascular wall (blue; collagen fibers; grey, autofluorescence of the extracellular matrix), see also **Online Movie XI.** The shown extended depth of field projections are derived from z-stacks with a total thickness of 24µm (step size = 2µm, total time window: 250s), Scalebar = 75 µm. (**C**) 3D reconstruction of an XYZ stack of the dataset in B, where the viewing angle was altered to mimic a transversal view on the vessel wall (blue-green) and the tracked adherent cell (green, red box). (**D**) Extended depth of field projection demonstrating myeloid cell crawling in close contact with the vessel wall in more detail (scalebar = 25µm). TRITC-dextran (orange) was used to label the blood stream. Total z-depth of the extended depth of field projection is ≈ 18µm (step size =2µm, total time window: 450s) (**Online Movie XII**). (**E**) 3D reconstruction of an XYZ stack of the same dataset, where the viewing angle was altered to mimic a transversal view on the vessel wall and adherent cells (green), collagen in the tunica adventitia (blue) and the lumen (red). Cells are crawling directly on the vessel wall since no dextran was detectable between myeloid cells and the wall. (**F**) Tracking of myeloid cells (depicted in the red box) over time using 3D isosurface rendering derived from z-stacks over time (see also **Online Movie XIII**). Scalebar = 25µm. Grey arrows (A, B, D, F) represent the direction of blood flow.

FIGURE 1

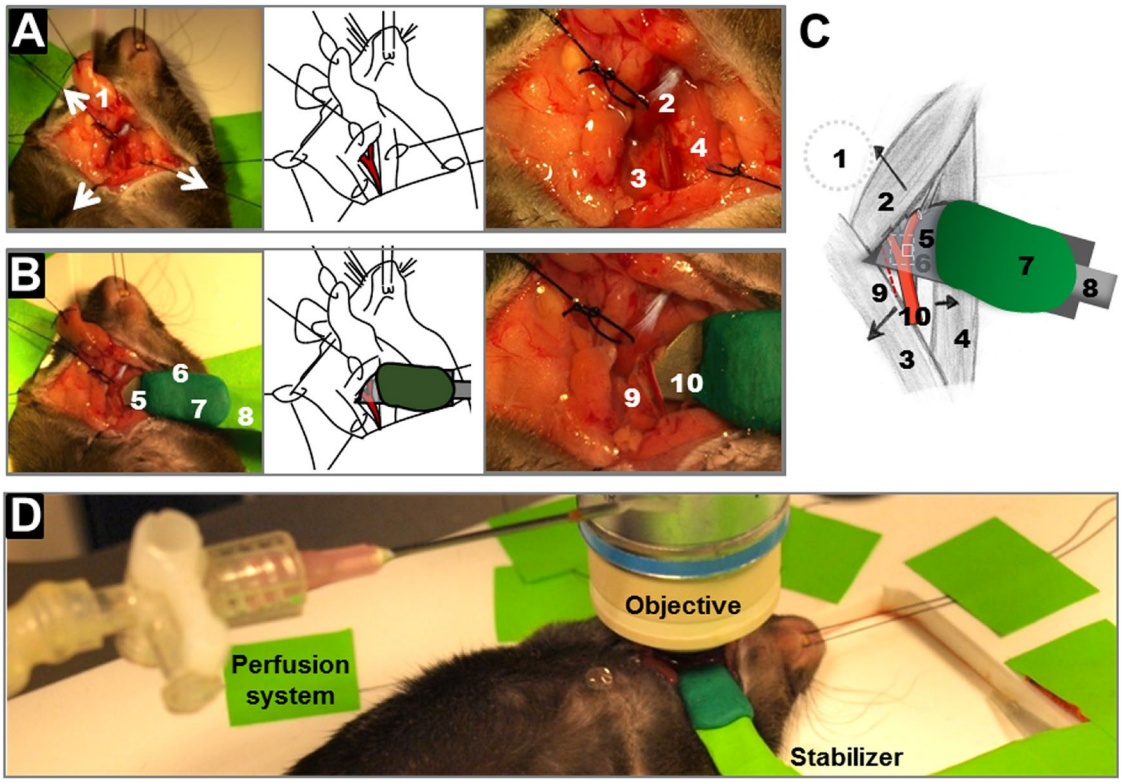
A
1
2
3
4
B
5
6
7
8
9
10
C
1
2
5
6
7
8
9
10
3
4
D
Objective
Perfusion system
Stabilizer

FIGURE 2

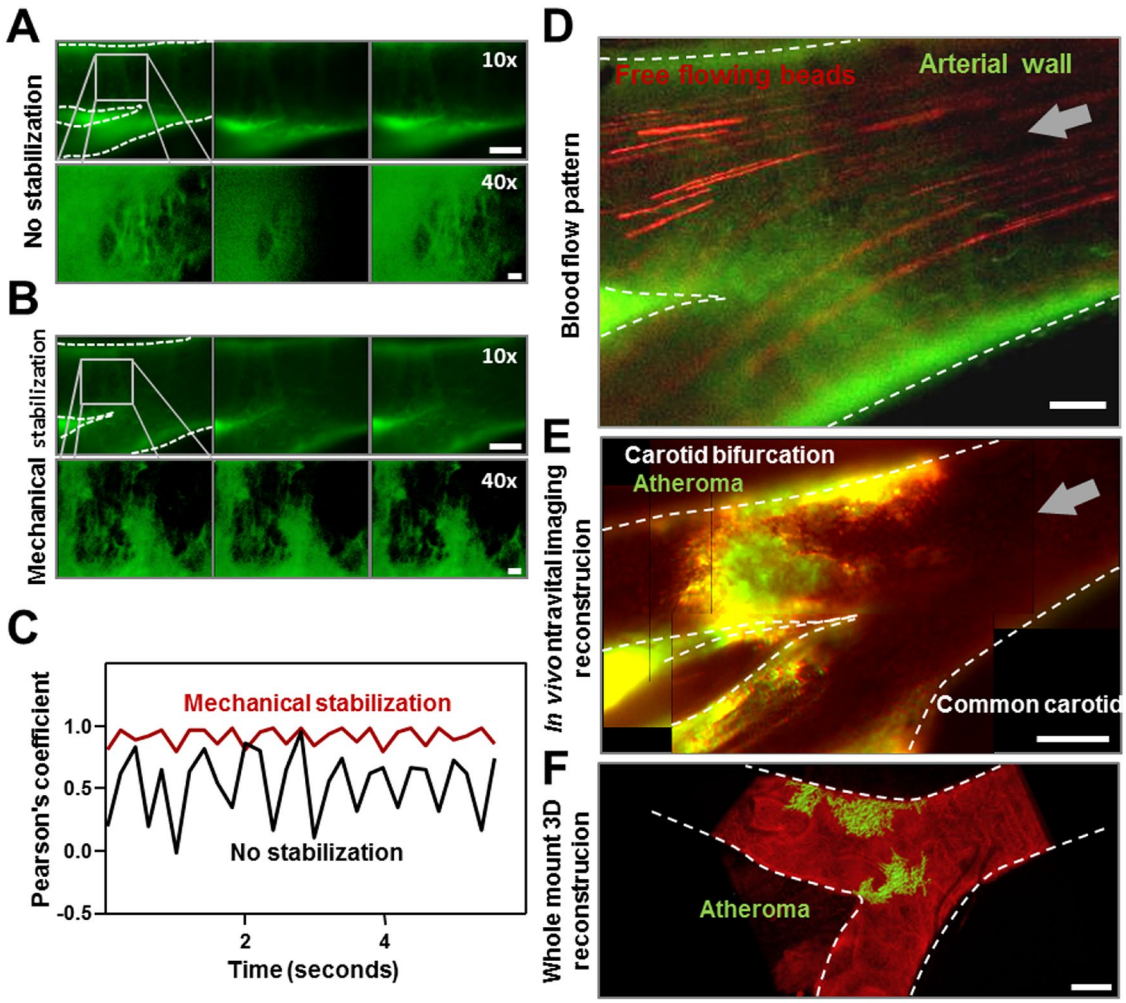
A
No stabilization
10x
40x
B
Mechanical stabilization
10x
40x
C
Pearson's coefficient
Mechanical stabilization
No stabilization
1.0
0.5
0.0
-0.5
2
4
Time (seconds)
D
Blood flow pattern
Free flowing beads
Arterial wall
E
In vivo ntravital imaging reconstrucion
Carotid bifurcation
Atheroma
Common carotid
F
Whole mount 3D reconstrucion
Atheroma

FIGURE 3

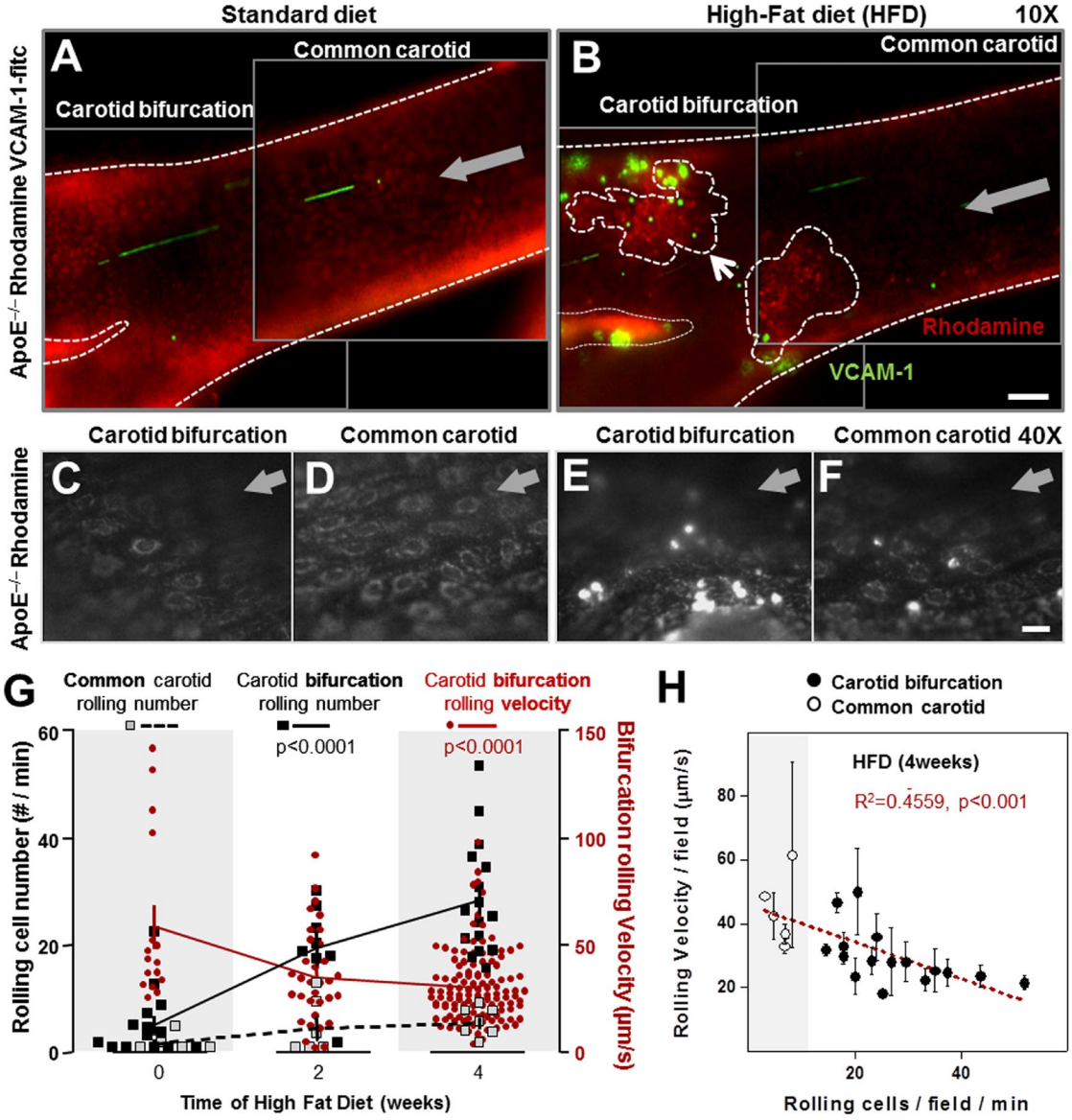
Standard diet
High-Fat diet (HFD)
10X
A
Common carotid
Carotid bifurcation
B
Common carotid
Carotid bifurcation
ApoE−/− Rhodamine VCAM-1-fitc
Rhodamine
VCAM-1
Carotid bifurcation
Common carotid
Carotid bifurcation
Common carotid 40X
C
D
E
F
ApoE−/− Rhodamine
G
Common carotid rolling number
Carotid bifurcation rolling number
Carotid bifurcation rolling velocity
p<0.0001
p<0.0001
Rolling cell number (# / min)
Bifurcation rolling Velocity (µm/s)
Time of High Fat Diet (weeks)
H
Carotid bifurcation
Common carotid
HFD (4weeks)
R²=0.4559, p<0.001
Rolling Velocity / field (µm/s)
Rolling cells / field / min

FIGURE 4

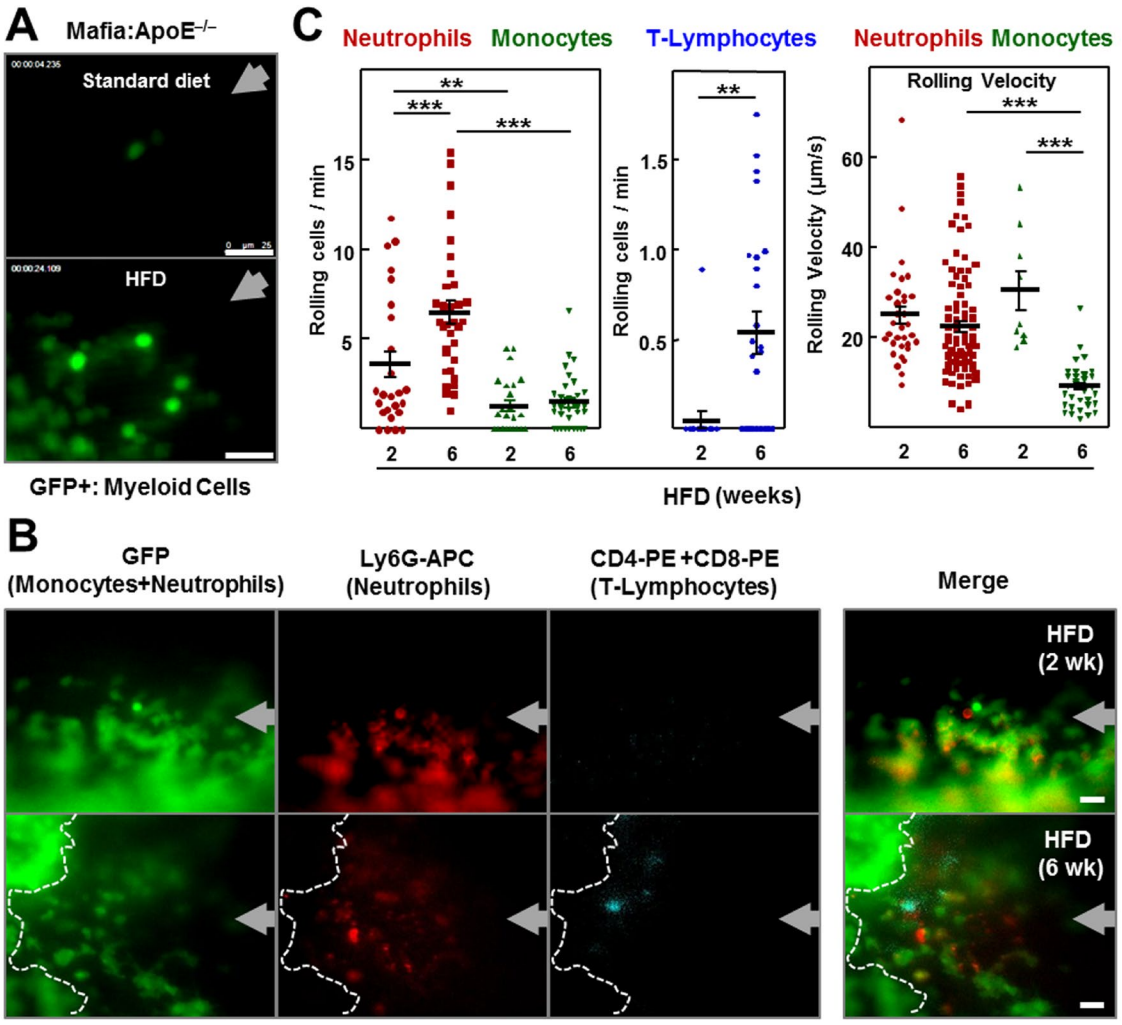
A
Mafia:ApoE−/−
Standard diet
HFD
GFP+: Myeloid Cells
C
Neutrophils
Monocytes
T-Lymphocytes
Neutrophils
Monocytes
Rolling cells / min
Rolling Velocity
Rolling Velocity (µm/s)
**
***
***
**
***
***
15
10
5
1.5
1.0
0.5
60
40
20
2
6
2
6
2
6
2
6
HFD (weeks)
B
GFP
(Monocytes+Neutrophils)
Ly6G-APC
(Neutrophils)
CD4-PE +CD8-PE
(T-Lymphocytes)
Merge
HFD
(2 wk)
HFD
(6 wk)

FIGURE 5

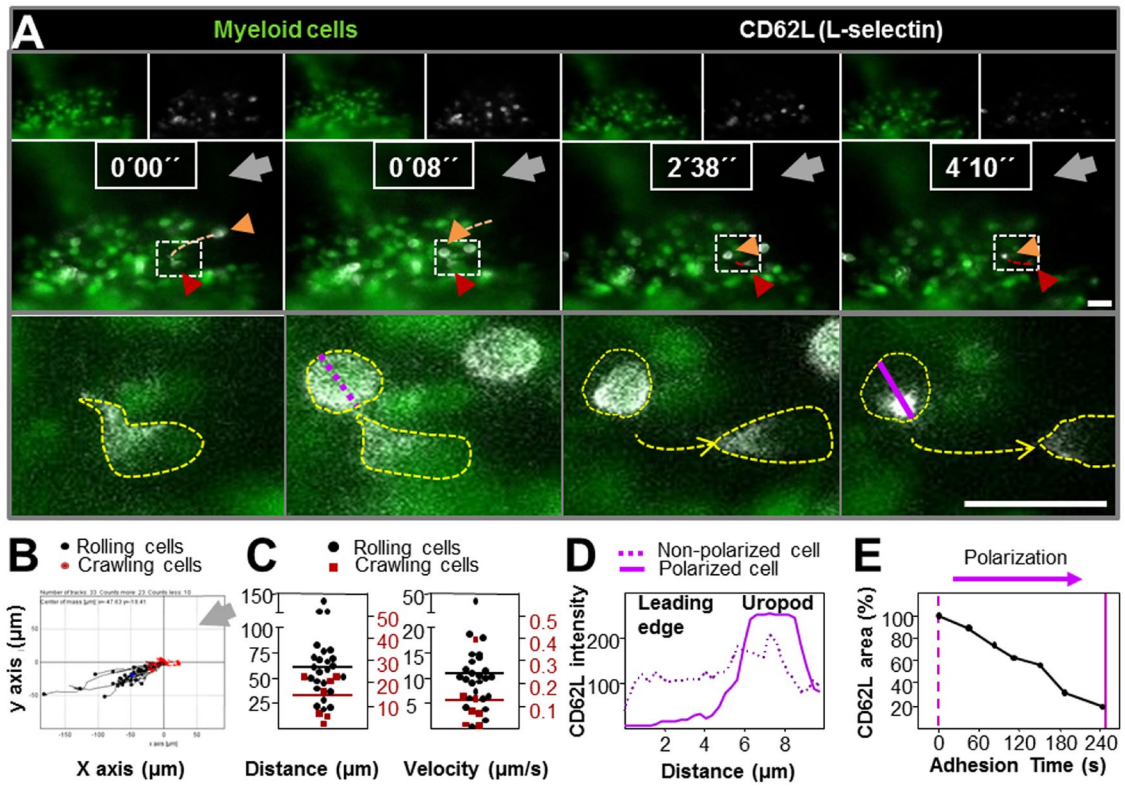
A
Myeloid cells
CD62L (L-selectin)
0´00´´
0´08´´
2´38´´
4´10´´
B
Rolling cells
Crawling cells
y axis (µm)
X axis (µm)
C
Rolling cells
Crawling cells
Distance (µm)
Velocity (µm/s)
D
Non-polarized cell
Polarized cell
Leading edge
Uropod
CD62L intensity
Distance (µm)
E
Polarization
CD62L area (%)
Adhesion Time (s)

FIGURE 6

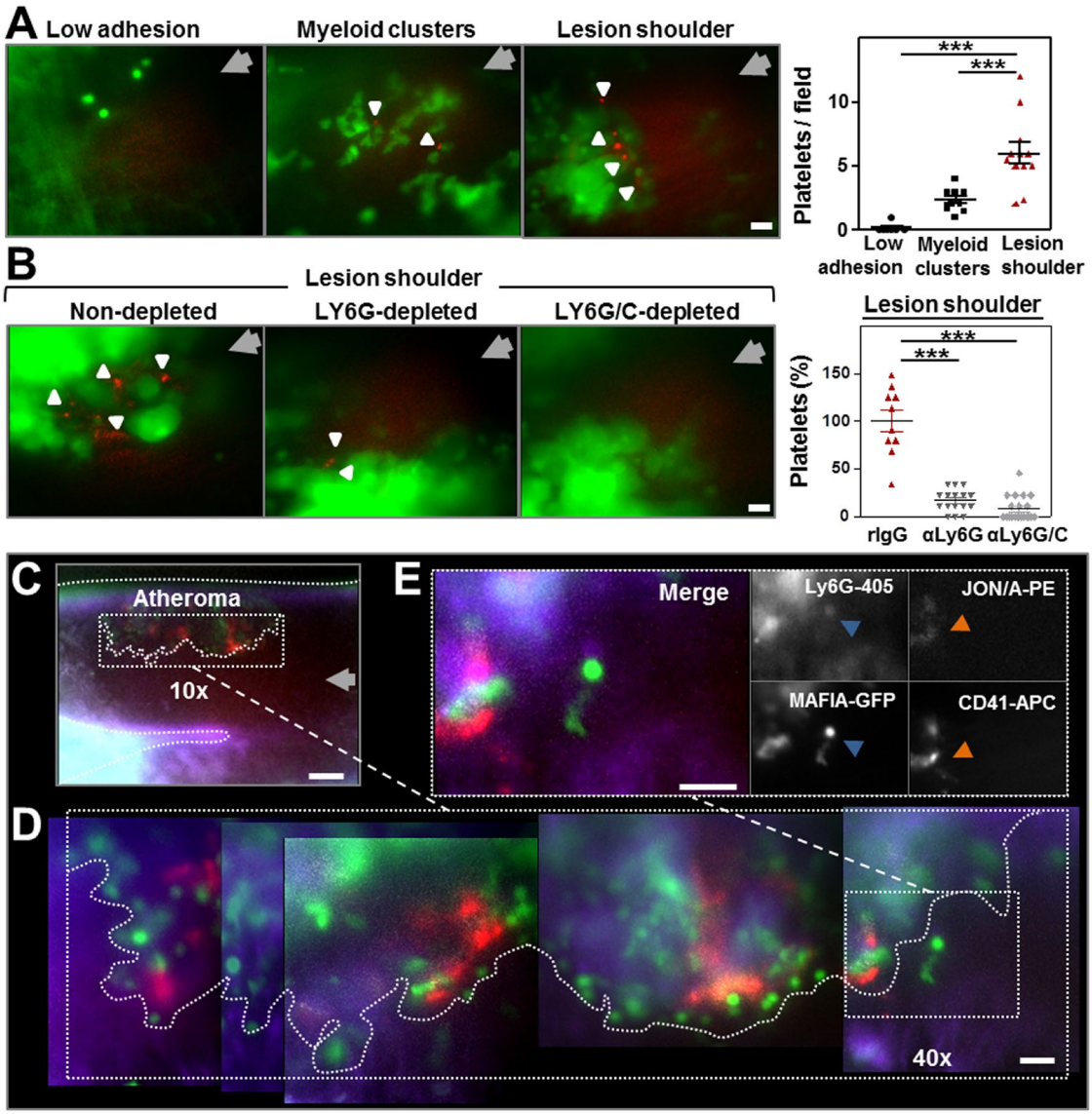
A
Low adhesion
Myeloid clusters
Lesion shoulder
Platelets / field
***
***
10
5
0
Low adhesion
Myeloid clusters
Lesion shoulder
B
Lesion shoulder
Non-depleted
LY6G-depleted
LY6G/C-depleted
Lesion shoulder
Platelets (%)
***
***
150
100
50
0
rIgG
αLy6G
αLy6G/C
C
Atheroma
10x
E
Merge
Ly6G-405
JON/A-PE
MAFIA-GFP
CD41-APC
D
40x

FIGURE 7

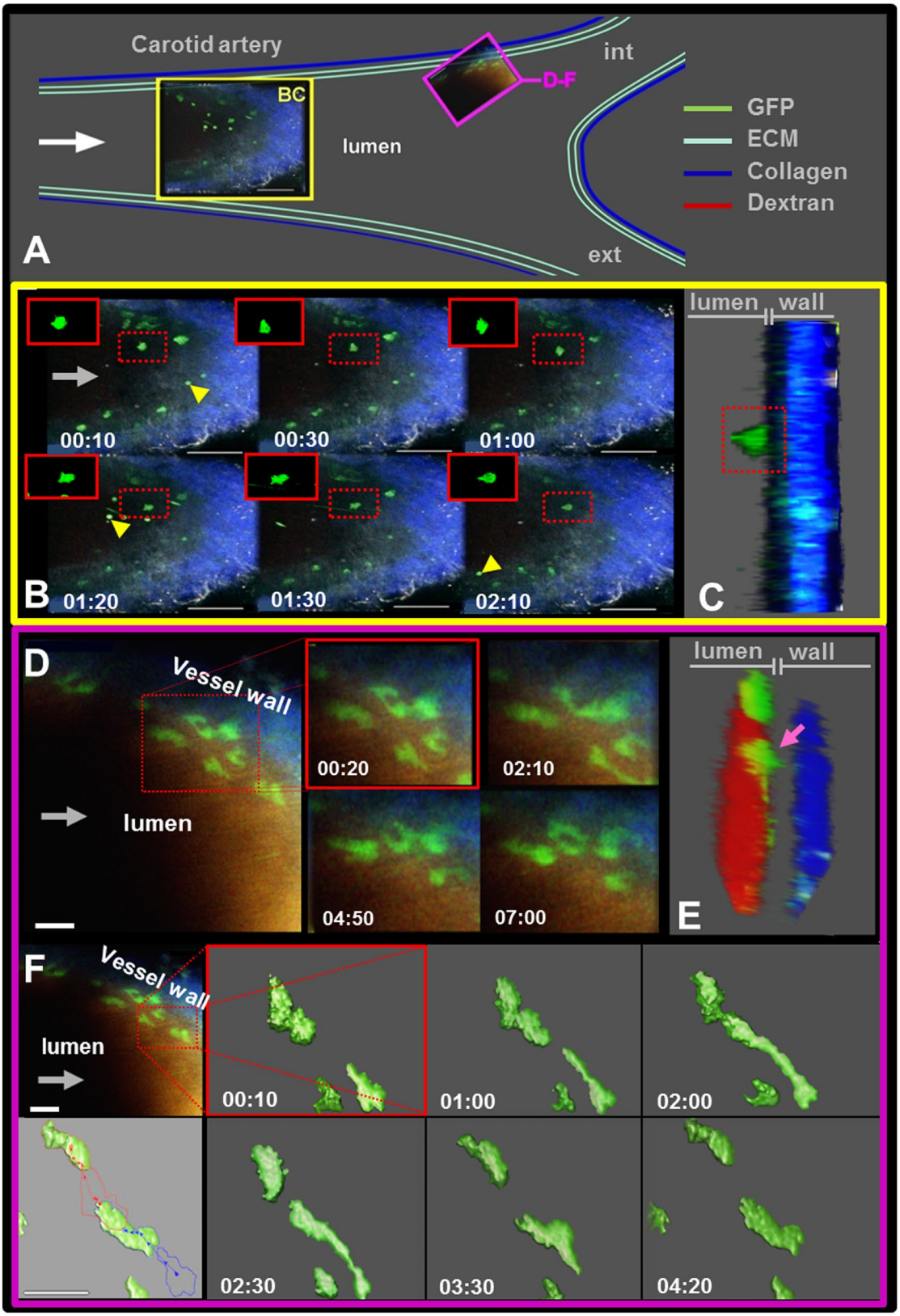
Carotid artery
int
BC
D-F
lumen
GFP
ECM
Collagen
Dextran
A
ext
00:10
00:30
01:00
lumen
wall
B
01:20
01:30
02:10
C
D
Vessel wall
00:20
02:10
lumen
04:50
07:00
lumen
wall
E
F
Vessel wall
lumen
00:10
01:00
02:00
02:30
03:30
04:20